Change Detection on Earth Surface by Biogeography-Based Optimized UNet from Multi-Temporal Hyperspectral Image

Bar, R. K.,[1*] Mukhopadhyay, S.[1] and Chakraborty, D.[2]
[1]Department of Computer Science and Engineering, Assam University, India, E-mail: rdhk_bar@yahoo.co.in*
[2]Regional Remote Sensing Centre-East, Indian Space Research Organization (ISRO), India
**Corresponding Author*

DOI: https://doi.org/10.52939/ijg.v21i3.4007

Abstract
Change Detection (CD) measures the identification of differences in the condition of living and non-living objects on the Earth's surface over time. Hyperspectral images (HSI) captured by satellites contain a vast amount of spectral information, offering ability to detect even subtle changes on the Earth's surface. The high dimensionality of HSI and computational complexity make this task challenging. In this research we introduce a novel framework, Biogeography-Based Optimized UNet Biogeography-Based Unet (BBOUNet) to extract distinctive features from the extensive HSI to identify change detection in multi-temporal hyperspectral satellite images. Here we present a differential pyramid that utilizes a pair of input images for the UNet architecture. A learning-based upsampling technique is employed to enhance intricacies of the change detection. To optimize the parameters within the UNet, we employ Biogeography Based Optimization. The results of experiments show that our method works better than traditional models for hyperspectral images, proving it to be more accurate.

Keywords: Biogeography Based Optimization, Change Detection, Earth Surface, Hyper Spectral Images, UNet

1. Introduction

Both living and non-living elements on the Earth's surface change over time. Plants, forests, and wildlife grow or decline, while cities, roads, and buildings expand. Natural elements like rivers, mountains, and soil also shift due to weather, erosion, and human activity. Monitoring these changes helps us understand how the planet is evolving and how we can better manage our environment. Change detection on the Earth's surface is important for tracking environmental changes like deforestation, urban growth, and the impact of natural disasters. It helps with urban planning, disaster management, and monitoring agriculture and climate change. This information is essential for protecting the environment and making informed decisions about land use and resource management. When Sunlight or other wave hit the Earth surface, different object like living-element and non-living element on earth surface interact with it differently. Satellite sensors capture reflection of this interaction data from the Earth's surface by detecting sunlight that bounces off objects like land, water and vegetation. The sensors measure the amount and type of light reflected back, allowing them to gather information about the materials and conditions on the ground.

This data helps in analyzing various features of the Earth's surface. Various hyperspectral imaging sensors are used for acquiring the HSIs, which help to differentiate the subtle changes from various ground objects [1]. The finding of high spectral information from HSIs is important in various applications like image classification, band selection, anomaly detection, change detection, hyperspectral unmixing, and so on [2]. The acquired HSI from remote sensors is a complex image that consists of multiple sub-bands, which are narrowly spaced [3]. In HSI, each band of a particular region captures the electromagnetic spectrum with multiple wavelengths [4]. Spectral information in hyperspectral images contains much more detailed data about a region than traditional multi-band images. While multi-band images capture a limited number of broad spectral bands, hyperspectral images record hundreds of narrow bands across the electromagnetic spectrum. This allows for more precise identification of materials, subtle differences in surface features, and changes over time, making it more informative for tasks like land use analysis, vegetation monitoring, and environmental changes [4].

Generally, HSIs are considered to be image cubes that contain hundreds of spatial images [5], where each image records the ground objects' responses at various wavelengths [6]. The range of HSI is spread from the visible range to infrared and ultraviolet [7]. These ranges of images are not visible to the human eye. The ground objects are identified by using the important information from the images [8].

The difference between the same ground objects is determined using the change detection process by the observation values at different time [9]. This is helpful in various implications such as environmental management, land cover mapping, and disaster monitoring [10]. Using ratios and image subtraction is an important method for detecting changes. By comparing images taken at different times, subtraction highlights the differences between them, making it easier to spot changes in the landscape, vegetation, or other features. Ratios, on the other hand, help in identifying subtle changes by comparing the intensity of specific wavelengths across images. Both techniques are effective in monitoring changes on the Earth's surface [11]. Change Vector Analysis (CVA) is the most commonly used unsupervised method that uses spectral vectors for performing subtraction [12]. The adaptive fusion strategy is utilized to identify the changes using a change detection map, where the spectral angle and change vector is included [13]. The training system is included in the supervised methods among the ground truth data [14]. Here, most pixels are designated as unchanged or changed [15].

Moreover, the labels and the remaining pixels are also learned. This detection process has effectively solved the imbalanced class problems. The active learning techniques are also explored to find the changes in detection by sharing a resemblance to the semi-supervised models. The band selection approach is also used to address the problem of change detection. But the subpixel level changes are not effectively handled by using the supervised learning-based approaches. To resolve the problems that occur in the conventional change detection in HIS, a new deep learning-based change detection scheme is developed to provide more accuracy. The contributions of the developed change detection scheme in HSI are summarized below:

- To introduce an efficient change detection mechanism in HSI to detect the subpixel level changes in HSI with high detection accuracy.
- To design a BBOUNet model for the detection of changes in HSI, where the activation function, hidden neuron count, and epochs in the UNet network are optimized using BBO to maximize the change detection accuracy.
- The efficiency of the developed model is revealed through various conventional change detection mechanisms according to several evaluation metrics.

The subsequent sections are structured to present the evolution of the HSI change detection mechanism based on the BBOUNet. In Section II, a comprehensive literature review is presented, highlighting various change detection mechanisms along with their associated challenges and distinguishing features. Moving forward, Section III offers a detailed exposition of the proposed methodology, providing insights into the structural aspects of the BBOUNet-based approach. The dataset used in the study and the results obtained from the experiments are discussed and analyzed in Section IV. This section sheds light on the performance evaluation and provides a thorough examination of the outcomes achieved through the BBOUNet's application in HSI change detection.

2. Literature Review

Traditional methods have limitations and need higher accuracy, so advanced deep learning techniques are becoming more popular. These techniques are especially useful for hyperspectral image analysis because they provide faster and more accurate segmentation. By using deep learning, we can reduce the time needed for segmentation, which makes tasks like disease diagnosis from satellite images more efficient. Overall, these new methods have the potential to greatly improve how we analyze satellite images, making results quicker and more accurate for important applications. Over the last few years, the advancement of deep learning has greatly progressive area of change detection algorithms [16] and [17] particularly in the domain of hyperspectral data. Existing hyperspectral change detection methods much rely on deep supervised learning [18] and [19], striking the use of labelled training data. While these high-quality training datasets offer precise supervision for model parameter training and yield impressive performance, their acquisition is labor-intensive and often challenging.

Consequently, addressing the issue of hyperspectral change detection without the heavy reliance on annotated labels has become a crucial goal in this area. Self-supervised learning [20] and [21] has emerged as a promising paradigm in machine learning, allowing models to learn feature representations from vast amounts of unlabelled data. It has gained significant attention, especially in natural image processing, where numerous SSL representation learning algorithms have been developed.

An influential form of semi-supervised learning is contrastive learning (CL) [22] which seeks to reduce the distance between pairs of positive samples while simultaneously increasing the separation among pairs of negative samples. CL has found practical utility in tasks such as change detection in multi-spectral optical and synthetic aperture radar (SAR) remote sensing [23] and [24]. Nevertheless, applying self-supervised learning to hyperspectral change detection encounters certain constraints. Current Self-supervised (SSL)-based change detection techniques predominantly revolve around the concept of instance discrimination. Specifically, multi temporal images are partitioned into patches to serve as inputs for the model. Subsequently, these patches undergo a transformation into feature vectors within the feature space to enable comparison. For this, the technique is confined to learning feature representations at the patch level, leading to outcomes in change detection that lack fine detail. The utilization of a spatial kernel filter, sliding across both horizontal and vertical dimensions in the 2D convolutional layer, concentrates on spatial information within individual channels, disregarding interrelationships among various spectral bands. This limitation hampers the effective utilization of spectral information.

In 2021, [25] developed a deep convolutional autoencoder for the detection of changes in the HSIs. This deep convolutional network was demonstrated for extracting the features from the image using fusion operation to detect the changes aroused in between the pair of bi-temporal-registered images. The features from the multiple receptive fields and successive levels have been considered for fusion operation. This method was completely unsupervised, and it was more elegant rather than the semi-supervised and supervised methods. Some amount of labelled information has been required for detecting the changes in HSIs. The empirical results have proven that the proposed method clearly outperformed the conventional models. In 2019, [26] presented a change detection approach in HSIs using CNN. The change detection maps from the traditional unsupervised change detection approaches were utilized for training the images. The noise present in the images was eliminated during end-to-end training. Here, FCN-based end-to-end deep network architecture has been designed to detect the changes based on the Hue Saturation Intensity (HSI) values by effectively learning the powerful features. The robust training was provided using the unsupervised noise modeling method. Finally, the effectiveness of the developed model was confirmed on three different datasets. In 2019, [27] focused on band-by-band pixel-based subtraction methods to find the changes in the present information for each band.

The Hyperspectral Change Vectors (HCVs) have been defined for all the multi-temporal images. Then, simplified the information changes from HCVs and then separately analyzed the radiometric information to create a quantized discrete representation. The hierarchical nature of the HSI changes has explored the discrete representations. Various kinds of changes were discriminated by using the tree representation. Two distinct datasets were used for testing the effectiveness of the developed model in terms of various evaluation metrics. In 2019, [28] presented a 2-D CNN-based change detection framework in HSIs. Here, the subpixel representation was integrated using a mixed-affinity matrix for mining more cross-channel gradient features and fusing multisource information. The discriminative features were learned from the multisource data for enhancing the generalization ability at a higher level, and the experimental results revealed that the developed model outperformed the traditional approaches. In 2022, [29] developed a Residual Self-Calibrated Network (RSCNet) for the detection of changes among HSIs. The inter-spectral and inter-spatial dependencies were exploited by using the developed RSCNet method. The complexity of the method also has been decreased with the usage of fewer extra parameters used in this model. The discriminative representations were created heterogeneously by introducing the self-calibrated convolution filters that might be integrated in the convolutional layer. Then, the richer information has been explicitly obtained from the response calibration operation.

The experimental results were demonstrated that the proposed RSCNet method has provided more accurate results than the baseline change detection approaches. The HSI along with the high spectral resolution has provided the spectral information over other remote sensing images like synthetic aperture radar images as well as multispectral images. One of the major difficulties in the HIS is defined as it is easily influenced by the noise at the time of image gathering process. Hence, it has shown low level depiction of HSIs are not discriminative in performing the task of change detection. Convolutional autoencoder [25] technique has safely claimed the feature extraction phase and also provided better performance over other models. It has also been utilized to minimize the noise effect. This technique has faced the difficulty on over fitting, and the label information in the dimensionality is minimized.

CNN [26] running-time of this technique is low, as well as the higher time efficient that enhances the performance of the model. It is considered as the powerful learning feature, which is robust on the training phase. But this technique has contained only a limited number of the dataset that has to be explored in terms of performance. Binary code words [27] the discrete depiction of the channel information, have been effective.

It is more complex due to maximized redundancy and dimensionality. The binary code-words that have been acquired to decrease the redundant information are not detailed. CNN [28] method is used to learn the series of more relevant features along with excellent robustness as well as generalization. The performance of the techniques is effective when analysed over conventional and newly constructed data. This method is not effective on processing the multisource information fusion. RSCNet [19] technique has the ability to encode the informative context that makes the model discriminative. It is regarded as generic as well as easily employed to standard layers without using the parameter. This technique has failed to perform the calibration process as well as it is cost effective. The dense skip structure utilized in Unet has proven to be highly effective in seamlessly integrating multilayer features. In the context of Change Detection, this technique becomes particularly valuable, as it addresses the challenge of dealing with hyperspectral images that exhibit significant variations in the scale of the changed regions [30]. The ability to effectively segment objects at different scales becomes paramount in this task. Remote sensing images often contain diverse scenes, with some regions undergoing minimal changes while others experience substantial transformations. Traditional segmentation methods may struggle to cope with such variability.

However, the dense skip connections employed by Unet enable the model to capture and utilize feature information at various levels, facilitating more accurate and robust object segmentation [31]. By fusing multilayer features effectively, Unet can adapt to the varying scales of changed regions of HSI, providing a powerful tool for precise and reliable Change Detection. This approach ensures that objects and changes, regardless of their size, are adequately identified and delineated, enhancing the overall performance and applicability of the segmentation model in remote sensing applications. Despite the advancements in change detection techniques, they still encounter certain constraints. Firstly, explicit difference representations, such as the approach used in [32], prove to be more advantageous than implicit difference presentations when it comes to extracting changing features. The utilization of explicit differential information enhances the model's ability to discern and capture subtle variations in the remote sensing images, leading to more effective detection of changes. Secondly, a common challenge in Change Detection is accurately segmenting the regions near the edges of the changed areas. Conventional methods often encounter difficulties in precisely identifying these edge regions, which can result in erroneous predictions. Recognizing this issue, we focused on refining the segmentation performance near these edges to reduce inaccuracies and minimize the likelihood of misclassifications. Addressing these limitations holds the key to further enhancing the performance of change detection from hyperspectral images.

3. Proposed Methodology

Taking the above limitations considerations into account, we have developed a novel Change Detection network called BBOUNet. This network leverages explicit difference representations to improve the extraction of changing features, allowing for more precise discrimination between changed and unchanged regions. Additionally, BBOUNet incorporates specialized mechanisms to address the inaccuracies in segmenting areas near the edges of changed regions, resulting in a more robust and reliable model for Change Detection tasks in remote sensing images. Moreover, it needs to increase the accuracy of the detection process. Therefore, a new change detection mechanism Biogeography-based optimized UNet (BBOUNet) is developed using deep learning in HSI. Taking the above limitations considerations into account, we have developed a novel Change Detection network called BBOUNet. This framework provide clear difference representations to enhance the ability to detect changes, making it easier to distinguish between areas that have changed and those that have remained the same. Additionally, BBOUNet incorporates specialized mechanisms to address the inaccuracies in segmenting areas near the edges of changed regions, making it a robust and more reliable model for detecting changes in remote sensing images. Moreover, it needs to increase the accuracy of the detection process. Therefore, a new change detection mechanism Biogeography-based optimized UNet (BBOUNet) is developed using deep learning in HIS. The BBOUNet architecture incorporates pyramid differential maps of two input images, which are the input for the UNet. To enhance the accuracy of change detection, a learning upsampling strategy is employed in the layer before prediction.

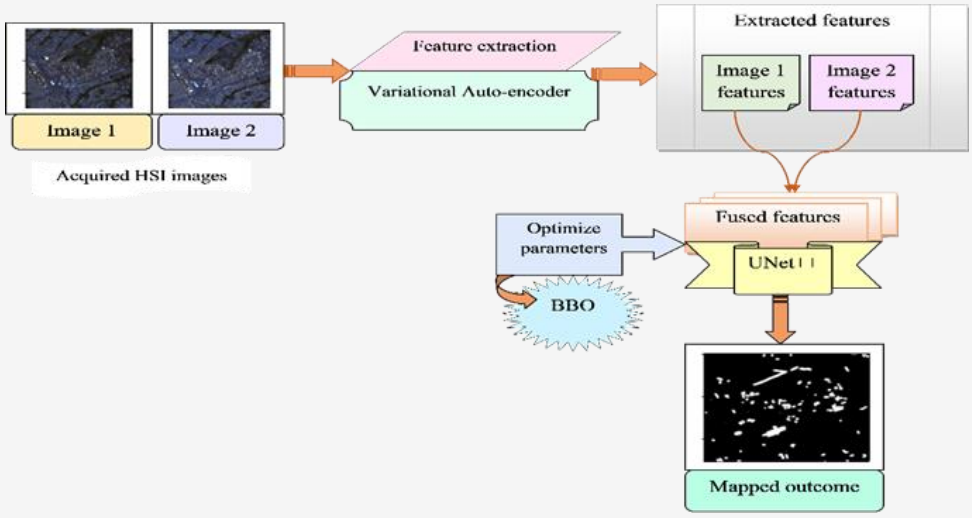

Figure 1: Proposed BBOUnet change detection framework

In contrast to traditional bilinear interpolation, the upsampling approach is highly effective at improving the detection of fine details, especially in areas around edges where changes occur. In this model we employed two upsampling strategies: bilinear interpolation and BBUpsampling. BBUpsampling is a novel learning-based technique that takes into account the correlation between pixel predictions. As a result, it is implemented to upsample the feature maps from Level 2 to Level 1, effectively improving the overall change detection outcomes. By adopting these upsampling strategies, the BBOUNet architecture achieves enhanced performance in accurately detecting and delineating changes in remote sensing images. The upsampling enhances edge detection in hyperspectral images by preserving sharp transitions and cleansing spatial-spectral details.

It treats edge pixels as high-priority regions, redistributing solutions to maintain boundary clarity while smoothing inconsistencies. By integrating spectral and spatial features, BBO reduces artifacts and dynamically adjusts resolution near edges, ensuring sharper and more accurate change detection. The structural description of this approach is given in Figure 1. The Hyperspectral images used for this study were collected from conventional databases. To capture features from images of different scales effectively, a variational autoencoder was employed to extract these features. Subsequently, the extracted features were fed into the change detection process, where the UNet method was utilized to achieve superior detection outcomes. To optimize the performance of the model, critical parameters, including activation attributes, hidden neurons, and epochs, were fine-tuned using the BBO (Biogeography-Based Optimization) algorithm. This optimization process aimed to maximize the precision rate of change detection. For ensuring the effectiveness of proposed framework, extensive experimental results were obtained and analyzed. These results were compared with various conventional change detection mechanisms, confirming the robustness and superiority of our approach in accurately detecting changes in the input remote sensing images.

3.1 Variational Autoencoder-based Feature Extraction

The variational autoencoder is utilized for extracting features from two images. From the spectral information, the latent space features are generated using this variational autoencoder, and the estimation of mean and variance values are important for providing high robustness. The appropriate features are effectively extracted using this variational autoencoder among HSIs. The need for a variational autoencoder is to insert the Gaussian noise at the output of encoders to provide more robust results after decoding. In HSIs, the latent embeddings always reside in low-dimensional space. The complexity due to the large dimensional vector is reduced using this variational autoencoder. For the given input y, the high-similarity sample $\hat{y}$ is obtained from the latent vector space, which is indicated by Lv. Here, the latent vector Lv is generated from the prior distribution p_d (Lv), and from the conditional distribution c_d ($y|Lv$), the expected sample is created. The posterior distribution is denoted by p_d ($Lv|y$), which is to be intractable.

In the variational autoencoder model, $C\delta(Lv|y)$ it is used for Gaussian distribution and the term δ is the encoder network parameter. The evidence of lower *EL* bound is introduced, which is shown in Equation 1:

$$EL = E_{c\delta\,(Lv|y)}\, p_d\,(y|Lv) - lkf\,[p_d\,(Lv|y), C\delta(Lv|y)$$

Equation 1

Here, the term $E_{c\delta\,(Lv|y)}\, p_d\,(y|Lv)$ denotes the generation probability of input *y*. The loss function value is indicated by the term *lkf*. Here, the generation probability is determined using the cross-entropy function. $p_d\,(y|Lv)$ is regarded as $\lambda(0,1)$ in Equation 2

$$\lambda(\eta, v^2) = \eta + \lambda(0,1) \times v$$

Equation 2

The second part is expressed in Equation 3.

$$Lkf\,[p_d\,(Lv|y), C\delta(Lv|y) = lkf\,[\lambda(0,1), \lambda(\eta, v^2)]$$

Equation 3

From the original data, the pure latent feature can be created that is considered as the mean value, and the standard deviation represents the additionally included Gaussian noise. The mean and the variances are indicated by the terms η and *v* respectively.

3.2 Optimised UNet for Change Detection

The extracted features from two images say Ms_x^{FS1} and Ms_y^{FS2} are given to the feature fusion process with the support of the UNet network [26]. This fused image is useful to get the changes between two images. It is adopted to predict the changes in different scales by fusing the extracted features. Multi-scale change features are effectively identified by using the developed network. The basic UNet structure consists of upsampling modules, down sampling modules, and dense skip connections between the paths and convolution units. The network structure can be conceptual and consists of five horizontal paths. All the paths consist of a different number of convolution units and all the convolution units have a unique number of feature maps. The output feature map of the convolutional unit is indicated by oz_{lk} where *l* denotes l_{th} path in down sampling and *k* is the l^{th} convolution unit, which is connected along with skip direction. This output feature map can be expressed in Equation 4.

$$OZ_{l,k} = \begin{bmatrix} cn\left(\downarrow\left(OZ_{l-lk}\right)\right), & k=1 \\ cn\left(\left[OZ_{l,k}\right]_{k=0}^{k=1} \uparrow \left(OZ_{l+1,k-1}\right)\right), & k>1 \end{bmatrix}$$

Equation 4

Here, ↑ (.) is the upsampling operation, *cn*(.) is the convolution unit operation, [.] is the operation of concatenation, ↓ (.) is the operation of downsampling. The feature maps attained from the 1^{st} convolution unit are considered as the input when satisfying the condition $k = 1$ in the $(l-1)^{th}$ path. The input consists of two parts when k>1, $\left[OZ_{lm}\right]_{m=0}^{m=1}$ are the concatenated features from the dense-cross layer and $OZ_{l+1,k-1}$ is the output attained from $k-1$ convolution unit. The change features are identified using the difference information from two input images. Hence, to highlight the changes in the model, the differential pyramidal maps are adopted in this network. From the previous scale, two feature maps are down-sampled and given to a convolutional unit. In this model, two input features are taken at different scales that represented by $MS^{FS1}, HS^{FS2} \in \Re^{Ht \times Wt \times \Im}$ and the two groups of feature maps are denoted by $Ft_l^{g1}, Ft_l^{g2} \in \Re^{3\left(Ht/2^l\right)\times\left(Wt/2^l\right)}$ the l^{th} layer of the differential pyramid. The spatial size of this pyramid is assumed as 0.5^l of the original input image. The feature maps Ft_l^{g1} and Ft_l^{g2} are evaluated using $cn\left(\downarrow\left(Ft_{l-1}^{g1}\right)\right)$ and $cn\left(\downarrow\left(Ft_{l-1}^{g2}\right)\right)$, respectively. The absolute difference map $\left|Ft_l^{g1} - Ft_l^{g2}\right|$ in l^{th} layer is determined. when $k = 1$, $l = 0$, the two input images are assumed as Ft_0^{g1} and Ft_{l0}^{g2}, the concatenation of the original two images is obtained, and it is indicated by $OZ_{l,k}$ which is expressed in Equation 5:

$$OZ_{l,k} = \begin{pmatrix} cn\left(\downarrow\left(OZ_{l-1,k}\right)\right)\left|Ft_l^{g1} - Ft_l^{g2}\right|, & k=1 \\ cn\left(\left[OZ_{l,k}\right]_{k=0}^{k=1} \uparrow \left(OZ_{l+1,k-1}\right)\right), & k>1 \end{pmatrix}$$

Equation 5

From this Equation 5, the feature map of the differential pyramid $\left|Ft_l^{g1} - Ft_l^{g2}\right|$ is served as one part of the input and hence, the network may integrate into the feature maps very effectively and pay attention to the change in area characteristics.

3.2.1 UNet based optimization

The UNet mechanism is used in the developed model to fuse the two images to detect the changes between the images very effectively. Here, the BBO is used to optimize the attributes like epochs, activation function, and hidden neuron count from the UNet. The main objective of this parameter optimization is to increase detection accuracy. The objective function is given in Equation 6:

$$BF = \begin{pmatrix} agr\min \\ EP_t^{UNet}, HT_q^{UNet}, AF_r^{UNet} \end{pmatrix} \left(\frac{1}{ACRY} \right)$$

Equation 6

Here, EP_t^{UNet} are the tuned epochs, HT_q^{UNet} are the tuned hidden neurons, and AF_r^{UNet} is the tuned activation function in UNet. The epochs are tuned at and also the hidden neurons are tuned at [5,255], and the activation functions are tuned at [50,100]. The term denotes the accuracy and the formula for accuracy is given in Equation 7.

$$ACRY = \frac{R_{Pt} + R_{Nt}}{R_{Pt} + R_{Nt} + L_{Pt} + L_{Nt}}$$

Equation 7

Here, the true negative and positive measures are denoted by R_{Pt} and R_{Nt} as well as the false negative and positive rates are represented by L_{Pt} and L_{Nt}, respectively. The diagrammatic representation of optimized UNet-based change map is represented in Figure 2.

3.2.2 Biogeography based optimization

BBO algorithm is used in the developed model to improve the detection performance during the detection of changes in HSI. It is used to optimize the parameters such as hidden neuron count, activation parameters and epochs in UNet to improve the precision of the developed framework. It is inspired by biogeography which learns the distribution of geographical information from biological organisms. The permutation of integers is used to represent the habitat in BBO. The BBO algorithm starts with the initialized habitat values. The permutation is generated randomly, and it avoids duplicate habitats during initialization in order to improve the diversity

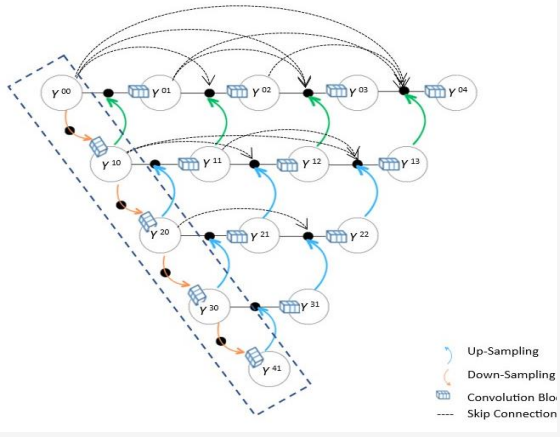

Figure 2: Unet architecture

[33]. The good habitats tend to distribute the features with the poor habitats. This distribution of features is accomplished using a migration mechanism, where the immigration rate γ_t and emigration rate ρ_t of the habitat is used for taking decision. The formula used to calculate immigration and emigration rates is given in Equation 8 and Equation 9:

$$\gamma_t = MI\left(1 - \frac{t}{n}\right)$$

Equation 8

$$\rho_t = \frac{EM_t}{n}$$

Equation 9

The rank of the habitat is indicated by *t*, the total number of habitats in the population, and is denoted by *n*, *MI* is the maximum immigration rate and *ME* is the maximum emigration rate. Each habitat has the associated probability in BBO, and the probability of mutation arising in the specific habitat is known as the mutation rate. Initially, the probability of species count is estimated using Equation 10:

$$P = \frac{u}{\sum_{h=1}^{P+1} u_n}$$

Equation 10

The formula of u and u_h are given in Equation 11 and Equation 12, respectively.

$$u = u_1, u_2, u_3, \ldots, u_{p+1}$$

Equation 11

$$u_h = \begin{Bmatrix} \frac{P!}{(P+1-h)!(h-1)!}, (h = 1,2,3,...,h) \\ u_{p+2-h} \quad , \left(h = \hat{h}+1,...,P+1\right) \end{Bmatrix}$$

Equation 12

Here, the term is estimated using Equation 13:

$$H = k + 0.5$$

Equation 13

Here, the term *k* is the initialized habitats in the search space. The mutation rate *Mut*(*R*) is inversely proportional to the species count probability and it is estimated using 14.

$$Mut(R) = MutMax\frac{1-P}{P_{max}}$$

Equation 14

In this, P_{max} gives the largest species count probability and *Mut*(*R*) represents the maximum

mutation rate. This mutation rate operator is used to maintain the feasibility of the solution. The diversity throughout the population is also enhanced by using this BBO.

4. Experimental Results

The proposed BBOUNet was subjected to a comprehensive evaluation to assess its effectiveness and practicality in detecting changes within multi-temporal hyperspectral images. To benchmark its performance, the BBOUNet was compared against six well established existing methods, namely CVA [34], PCA-CVA [34], and IR-MAD [35], UTBNet [36], Fisher-PSO [37] supervised approaches such as FCN [26], and GETNET [28].

The comparison was conducted using three distinct pairs of hyperspectral images. By conducting such a thorough assessment, researchers aimed to determine how the BBOUNet performed in relation to these state-of-the-art methods, thereby providing valuable insights into its capabilities and potential applications of change detection in complex HSI data

4.1 Dataset

In our experiments, we utilized three publicly available datasets obtained from Hyperion sensor. This sensor offers a total of 242 spectral bands, covering a wavelength range between 400 *nm* and 2500 *nm*. The sensor has a spectral resolution of approximately 10 meters and a spatial resolution of around 30 meters. Figure 3(a) and Figure 3(d) depict the Farmland dataset. The dataset comprises two temporal hyperspectral images, captured on May 3, 2006, and April 23, 2007, respectively. The primary setting depicts a Yancheng, Jiangsu Province, China, farmland, spanning an area of 450 × 140 pixels. Following the removal of bands with inadequate signal-noise ratios, 155 channels were kept for subsequent analysis. In our experiment, we are using atmospheric-corrected and pre-processed data, so we have not applied any noise handling mechanisms at this stage The noteworthy fluctuations observed in the dataset are a result of the seasonal shifts i

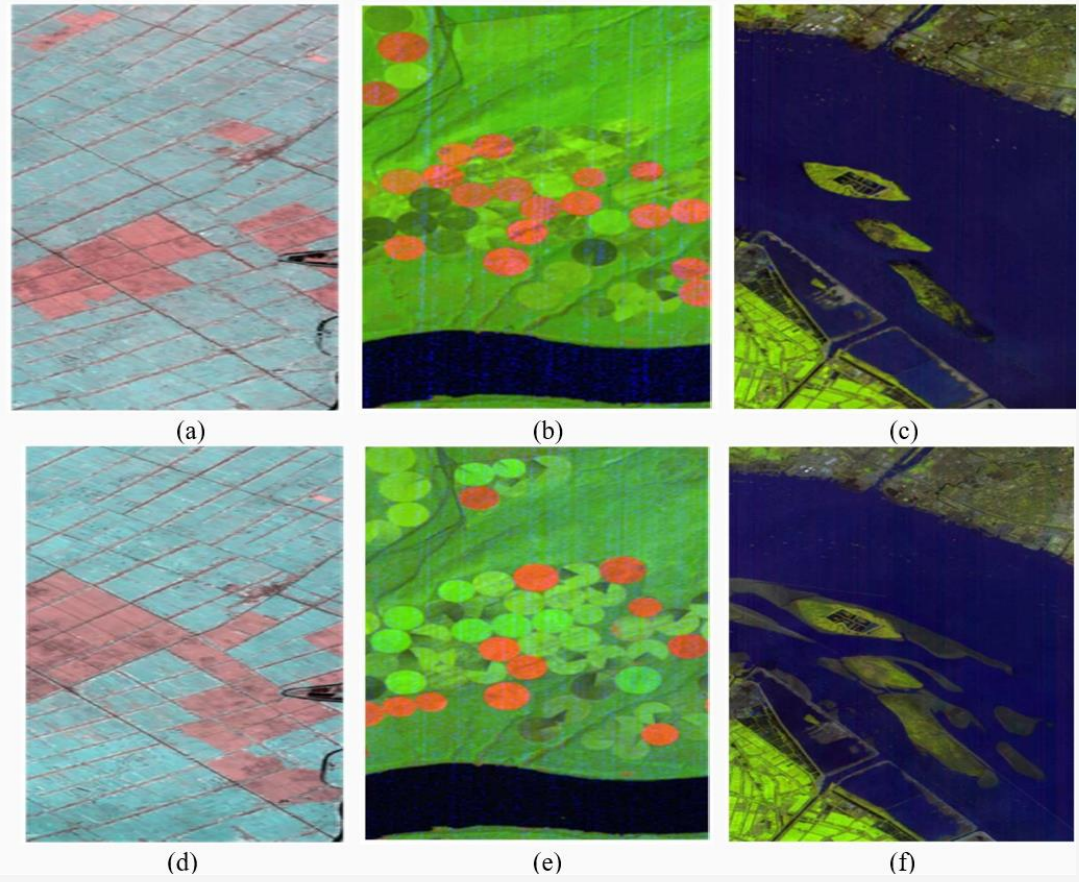

Figure 3: False Color Representation of three dataset:
(a) Farmland dataset (May 2006) (b) Hermiston dataset (May 2004) (c) River dataset (May 20) (d)Farmland dataset (23 April 2007) (e) Hermiston dataset (May 2007) (f) River dataset (December 2013)

The Hermiston dataset, displayed in Figure 3(b) and Figure 3(e) comprises two hyperspectral data taken on May 1, 2004 and another was taken on May 8, 2007. Main imagery showcases circular irrigation areas and the rivers within the city of Hermiston, USA. The dataset covers an expanse of 390×200 pixels. Following the removal of noise, a total of 163 bands were chosen for further analysis. Similar to the previous dataset, the main variations in the Hermiston dataset can be attributed to the seasonal changes in crops. The River dataset, illustrated in Figure 3(c) and Figure 3(f) consists of two images. First one was taken on May 3, 2013 and the second one was taken on December 31, 2013. The primary scenes captured depict residential areas and rivers located in Jiangsu Province, China, encompassing a total of 463×241 pixels. Following the removal of noise, a total of 167 bands were chosen for further analysis. The primary change observed in this dataset is the presence of sediment in the rivers and residential areas, which serves as the main differentiating factor. To enhance the convergence speed of our model, we performed normalization on the three datasets, scaling the values to a range between one and zero. Furthermore, to enhance the training dataset, we divided every HSI into sub-images of dimensions 32×32 pixels, using a step size of 8. Corresponding ground truth boundaries were also cropped accordingly to align with the sub-images. The sub-images obtained from the two temporal datasets were combined, shuffled, and utilized as training data for the network. Additionally, during the training process, these sub-images underwent random rotations, vertical flips, and horizontal flips as supplementary data augmentation techniques. In this section, we conducted a series of comprehensive experiments to validate the efficacy of the proposed method.

4.2 Discussion of Results

Our goal was to compare it against various change detection methods like unsupervised approaches CVA [34], PCA-CVA [34], IRMAD [35], and a Particle Swarn Optimization Fisher-PSO [37], and some supervised approaches such as FCN [26], GETNET [28] and UTBNet [36]. As demonstrated in Figure 4, the CVA, PCA-CVA, FCN, GetNet and UTBNet[36] results reveal a lot of white pixels in unaltered road regions when compared to the ground truth in case of Farmland

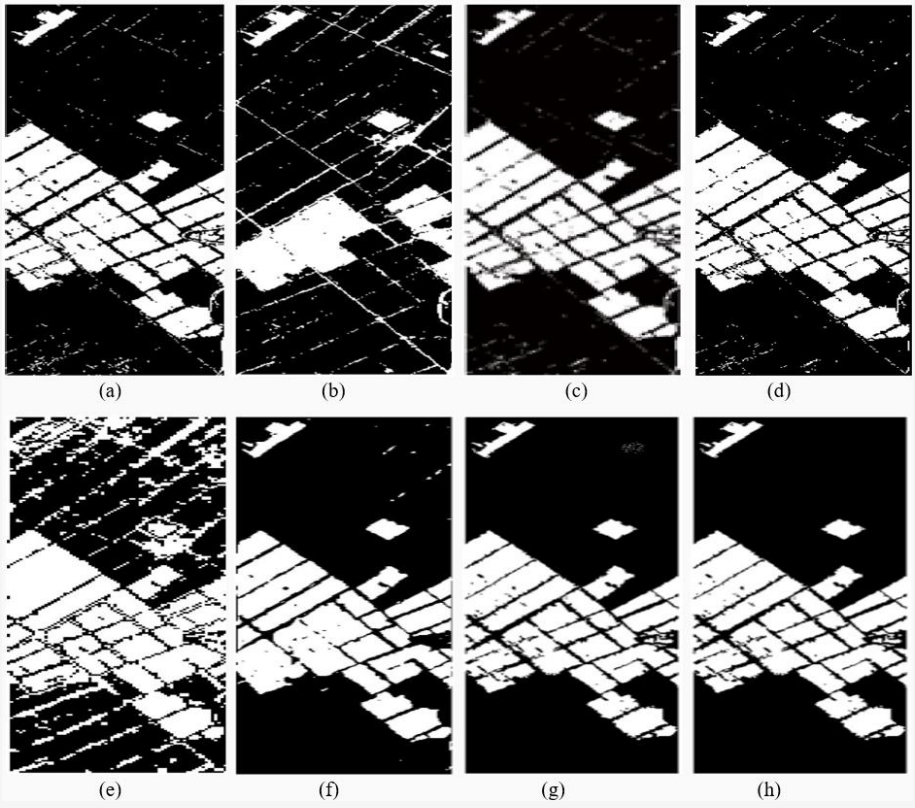

Figure 4: Binary change map of the dataset of farmland:
(a) CVA (b)PCA-CVA (c)IR-MAD (d)FCN (e)GetNet (f) UTBANet (g)Proposed method (h)Ground truth

Table 1: Change detection accuracy results of farmland dataset

Method	Overall Accuracy	Kappa Coefficient	Precision (%)	Recall (%)
CVA	0.949	0.882	79.53	78.33
PCA-CVA	0.965	0.318	79.01	79.31
IR-MAD	0.953	0.919	80.55	79.97
FCN	0.965	0.938	82.61	80.41
GetNet	0.978	0.957	81.82	79.83
UTBA	0.960	0.917	82.80	81.11
Fisher-PSO	0.945	0.848	80.23	80.53
Proposed	**0.987**	**0.967**	**83.36**	**82.63**

Table 2: Change detection accuracy results of Hermiston dataset

Method	Overall Accuracy	Kappa Coefficient	Precision (%)	Recall (%)
CVA	0.969	0.878	79.53	78.33
PCA-CVA	0.665	0.299	79.01	79.31
IR-MAD	0.772	0.403	80.55	79.97
FCN	0.792	0.682	82.61	80.41
GetNet	0.824	0.735	81.82	79.83
UTBA	0.979	0.929	82.82	81.11
Fisher-PSO	0.967	0.910	81.01	80.22
Proposed	**0.985**	**0.9301**	**83.36**	**82.63**

The mis judgment of unaltered pixels results in their erroneous classification as modified pixels, leading to false alarms. The performance of IR-MAD was unsatisfactory, as it exhibited numerous instances of noise across various types. In the case of GetNet, a significant false alarm area was observed in the top left corner of the output. The metrics for these methods are presented in Table 1. Our method outperformed the others, achieving the highest values across all five metrics: an Overall Accuracy of 0.987, Kappa Coefficient as 0.967, % of precision as 83.36 and % of Recall as 82.63 for the farmland data set.

While CVA successfully detected the majority of changed region, it also exhibited mis judgments by incorrectly identifying certain unchanged areas. Both FCN and PCA-CVA algorithms made mistake of detecting the river as a changed area. Furthermore, the performance of IR-MAD on this dataset was subpar, leading to the generation of various types of noise in the results. The Proposed method demonstrates the highest level of consistency with the ground truth. According to Figure 5, our method exhibits greater accuracy in detecting changed irrigation areas, without any noticeable false alarm pixels. Similar trend of result is observed for the river dataset also which is demonstrated in Figure 6. The outcomes of all methods are presented in Table 2, which highlights a problem with the PCA-CAV approach. This particular method shows a significant number of false alarm pixels, resulting in a KC value of only 0.299. Table 2 displays the quantitative indicators for all methods for Hermiston dataset. In Table 3, the comparative accuracy study is shown when the experiment is done with the revie dataset.

During the analysis using the PCA-CVA method, an incorrect identification of the river as a changed area was observed. This misclassification could potentially be attributed to the less signal-noise ratio prevalent in the river area, leading to misleading results. On the other hand, the IR-MAD method faced difficulties in detecting the changed region located in the middle of the river. Despite its ability to identify changes in various other areas, the specific characteristics of the changed region within the river seemed to pose challenges for the IR-MAD algorithm. These findings highlight the limitations of these methods in accurately detecting changes in complex environments such as river regions. Further improvements or alternative approaches may be required to address these challenges and enhance the accuracy of change detection in similar scenarios. The obtained results demonstrate that both the CVA method and our proposed method show a closer resemblance to the ground truth in terms of change detection.

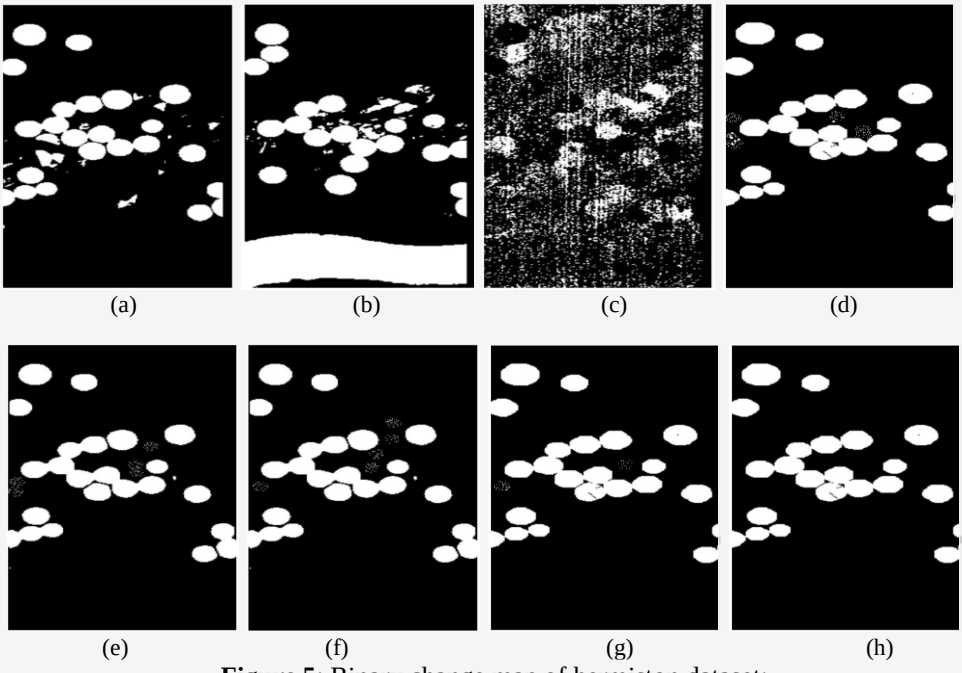

(a) (b) (c) (d)

(e) (f) (g) (h)

Figure 5: Binary change map of hermiston dataset:
(a)CVA (b)PCA-CVA (c)IR-MAD (d)FCN (e)GetNet (f) UTBANet (g)Proposed method (h)Ground truth

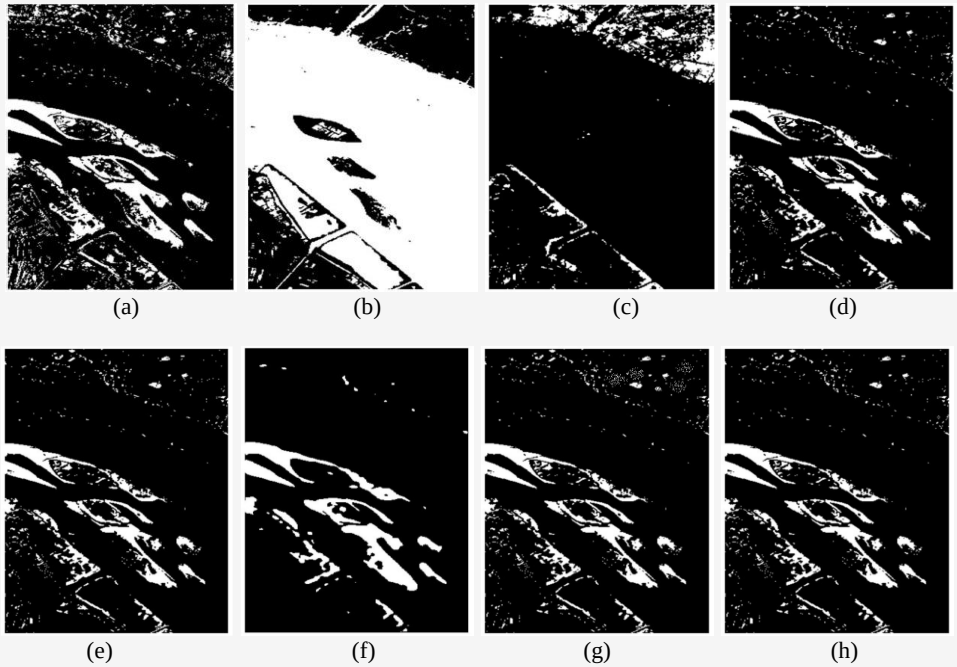

(a) (b) (c) (d)

(e) (f) (g) (h)

Figure 6: Binary change map of river dataset:
(a)CVA (b)PCA-CVA (c)IR-MAD (d)FCN (e)GetNet (f) UTBANet (g)Proposed method (h)Ground truth

However, when compared to CVA, our method exhibits a lower number of false alarm pixels, indicating its improved accuracy in detecting changes. On the other hand, the UTBANet method faced limitations as it failed to detect some of the small changed targets that were successfully identified by our proposed method.

This indicates the effectiveness of our approach in capturing subtle changes that may have been missed by other methods. These findings highlight the advantages of our method over existing techniques and its potential for enhanced change detection in various applications.

Table 3: Change detection accuracy results of river dataset

Method	Overall Accuracy	Kappa Coefficient	Precision (%)	Recall (%)
CVA	0.939	0.702	79.53	78.33
PCA-CVA	0.330	0.102	79.01	79.31
IR-MAD	0.865	0.084	80.55	79.97
FCN	0.871	0.689	82.61	80.41
GetNet	0.889	0.710	81.82	79.83
UTBA	0.949	0.718	82.8	81.11
Fisher-PSO	0.921	0.714	81.84	80.17
Proposed	**0.954**	**0.737**	**83.51**	**82.52**

5. Conclusion

In this research paper, we introduced a new version of the UNet architecture called "BBOUNet" by incorporating a Biogeography-Based Optimization (BBO) approach. Our proposed models are evaluated using three different image datasets: one of farmland with mostly living elements, another of irrigated land with a moderate amount of living elements, and a third of a riverside area with fewer living elements. Using the full range of spectral bands in hyperspectral images for change detection ensures that no valuable data is lost, as compared to band reduction methods. While band reduction can simplify data and improve processing time, it may result in the loss of subtle spectral features that are crucial for detecting small or localized changes. The high spectral resolution provides better differentiation between classes or subtle changes in the environment. This increased spectral detail helps improve the accuracy of change detection models, as they can capture more comprehensive information about spectral variations across the entire image. The experimental results clearly demonstrated that the BBOUNet model worked much better than other methods. This was true for all three datasets tested, showing its strong performance in comparison to existing techniques. Also, by using a Biogeography-Based approach for deep supervision, we were able to make better with only a small drop in performance. It may be noted that out of three different datasets. The dataset having considerable amount of living-element give better accuracy than another image.

References

[1] Liu, S., Bruzzone, L., Bovolo, F., Zanetti, M. and Du, P., (2015). Sequential Spectral Change Vector Analysis for Iteratively Discovering and Detecting Multiple Changes in Hyperspectral Images. *IEEE Transactions on Geoscience and Remote Sensing*, Vol. 53(8), 4363-4378. https://doi.org/10.1109/TGRS.2015.2396686.

[2] Ou, X., Liu, L., Tu, B., Zhang, G. and Xu, Z., (2022). A CNN Framework with Slow-Fast Band Selection and Feature Fusion Grouping for Hyperspectral Image Change Detection. *IEEE Transactions on Geoscience and Remote Sensing*, Vol. 60, 1-16. https://doi.org/10.1109/TGRS.2022.3156041.

[3] Ertu¨rk, A. and Plaza, A., (2015). Informative Change Detection by Unmixing for Hyperspectral Images. *IEEE Geoscience and Remote Sensing Letters*, Vol. 12(6), 1252–1256. https://doi.org/10.1109/LGRS.2015.2390973.

[4] Ertu¨rk, A., (2018). Unmixing Based Change Detection for Hyperspectral Images with Endmember Variability. In 2018 9th Workshop on *Hyperspectral Image and Signal Processing: Evolution in Remote Sensing (WHISPERS*), 1–5. https://doi.org/10.1109/WHISPERS.2018.8747255.

[5] Liu, S., Bruzzone, L., Bovolo, F. and Du, P., (2014). Hierarchical Unsupervised Change Selection in Multitemporal Hyperspectral Images. *IEEE Transactions on Geoscience and Remote Sensing*, Vol. 53(1), 244–260. https://doi.org/10.1109/TGRS.2014.2321277.

[6] Zhou, J., Kwan, C., Ayhan, B. and Eismann, M. T., (2016). A Novel Cluster Kernel Rx Algorithm for Anomaly and Change Detection Using Hyperspectral Images. *IEEE Transactions on Geoscience and Remote Sensing*, Vol. 54(11), 6497–6504. https://doi.org/10.1109/TGRS.2016.2585495.

[7] Zhan, T., Sun, Y., Tang, Y., Xu, Y. and Wu, Z., (2021). Tensor Regression and Image Fusion-Based Change Detection Using Hyperspectral and Multispectral Images. *IEEE Journal of Selected Topics in Applied Earth Observations and Remote Sensing*, Vol. 14, 9794–9802. https://doi.org/10.1109/JSTARS.2021.3115345

[8] Hu, M., Wu, C., Zhang, L. and Du, B., (2021). Hyperspectral Anomaly Change Detection Based on Autoencoder. *IEEE Journal of Selected Topics in Applied Earth Observations and Remote Sensing*, Vol. 14, 3750-3762. https://doi.org/10.1109/JSTARS.2021.3066508

[9] Gong, M., Jiang, F., Qin, A. K., Liu, T., Zhan, T., Lu, D., Zheng, H. and Zhang, M., (2021). A Spectral and Spatial Attention Network for Change Detection in Hyperspectral Images. *IEEE Transactions on Geoscience and Remote Sensing*, Vol. 60, 1–14. https://doi.org/10.1109/TGRS.2021.3139077.

[10] Eismann, M. T., Meola, J. and Hardie, R. C., (2007). Hyperspectral Change Detection in the Presence of Diurnal and Seasonal Variations. *IEEE Transactions on Geoscience and Remote Sensing*, Vol. 46(1), 237–249. https://doi.org/10.1109/TGRS.2007.907973.

[11] Hou, Z., Li, W., Li, L., Tao, R. and Du, Q., (2021). Hyperspectral Change Detection Based on Multiple Morphological Profiles. *IEEE Transactions on Geoscience and Remote Sensing*, Vol. 60, 1–12. https:10.1109/TGRS.2021.3090802.

[12] Akgun, T., Altunbasak, Y. and Mersereau, R. M., (2005). Super-Resolution Reconstruction of Hyperspectral Images. *IEEE Transactions on Image processing*, Vol. 14(11), 1860–1875. https://doi.org/10.1109/TIP.2005.854479.

[13] Liu, S., Bruzzone, L., Bovolo, F. and Du, P., (2016). Unsupervised Multitemporal Spectral Unmixing for Detecting Multiple Changes in Hyperspectral Images. *IEEE Transactions on Geoscience and Remote Sensing*, Vol. 54(5), 2733–2748. https://doi.org/10.1109/TGRS.2015.2505183.

[14] Chang, M., Meng, X., Sun, W., Yang, G. and Peng, J., (2021). Collaborative Coupled Hyperspectral Unmixing Based Subpixel Change Detection for Analyzing Coastal Wetlands. *IEEE Journal of Selected Topics in Applied Earth Observations and Remote Sensing*, Vol 14, 8208-8224. https://doi.org/10.1109/JSTARS.2021.3104164

[15] Eismann, M. T., Stocker, A. D. and Nasrabadi, N. M., (2009). Automated Hyperspectral Cueing for Civilian Search and Rescue. *Proceedings of the IEEE*, Vol. 97(6), 1031–1055. https://doi.org/10.1109/JPROC.2009.2013561.

[16] Shi, C., Zhang, Z., Zhang, W., Zhang, C. and Xu, Q., (2022). Learning Multiscale Temporal–Spatial–Spectral Features Via Multipath Convolutional LSTM Neural Network for Change Detection with Hyperspectral Images. *IEEE Transactions on Geoscience and Remote Sensing*, Vol. 60, 1–16. https://doi.org/10.1109/TGRS.2022.3176642.

[17] Yang, Y., Qu, J., Xiao, S., Dong, W., Li, Y. and Du, Q., (2022). A Deep Multiscale Pyramid Network Enhanced with Spatial–Spectral Residual Attention for Hyperspectral Image Change Detection. *IEEE Transactions on Geoscience and Remote Sensing*, Vol. 60, 1–13. https://doi.org/10.1109/TGRS.2022.3161386.

[18] Bai, T., Wang, L., Yin, D., Sun, K., Chen, Y., Li, W. and Li, D., (2022). Deep Learning for Change Detection in Remote Sensing: A Review. *Geo-spatial Information Science*, 1–27. https://doi.org/10.1080/10095020.2022.2085633.

[19] Wang, L., Wang, L., Wang, Q. and Bruzzone, L., (2022a). Rscnet: A Residual Self Calibrated Network for Hyperspectral Image Change Detection. *IEEE Transactions on Geoscience and Remote Sensing*, Vol. 60, 1–17. https://doi.org/10.1109/TGRS.2022.3177478.

[20] Ericsson, L., Gouk, H. and Hospedales, T. M., (2021). How Well Do Self-Supervised Models Transfer? *In Proceedings of the IEEE/CVF Conference on Computer Vision and Pattern Recognition*, 5414–5423.

[21] Wang, Y., Albrecht, C. M., Braham, N. A. A., Mou, L. and Zhu, X. X., (2022). Self-Supervised Learning in Remote Sensing: A Review. *IEEE Geoscience and Remote Sensing Magazine*, Vol. 10(4), 213-247. https://doi.org/10.1109/MGRS.2022.3198244.

[22] Jaiswal, A., Babu, A. R., Zadeh, M. Z., Banerjee, D. and Makedon, F., (2020). A Survey on Contrastive Self-Supervised Learning. *Technologies*, Vol. 9(1). https://doi.org/10.3390/technologies9010002.

[23] Shi, Q., Liu, M., Li, S., Liu, X., Wang, F. and Zhang, L., (2021). A Deeply Supervised Attention Metric-Based Network and an Open Aerial Image Dataset for Remote Sensing Change Detection. *IEEE Transactions on Geoscience and Remote Sensing*, Vol. 60, 1–16. https://doi.org/10.1109/TGRS.2021.3085870.

[24] Sun, Y., Lei, L., Li, X., Tan, X. and Kuang, G., (2021). Structure Consistency-Based Graph for Unsupervised Change Detection with Homogeneous and Heterogeneous Remote Sensing Images. *IEEE Transactions on Geoscience and Remote Sensing*, Vol. 60, 1–21. https://doi.org/10.1109/TGRS.2021.3053571.

[25] Chakraborty, D. and Ghosh, A., (2021). Unsupervised Change Detection in Hyperspectral Images Using Feature Fusion Deep Convolutional Autoencoders. *arXiv preprint arXiv*:2109, 04990.

[26] Li, X., Yuan, Z. and Wang, Q., (2019). Unsupervised Deep Noise Modeling for Hyperspectral Image Change Detection. *Remote Sensing*, Vol. 11(3). https://doi.org/10.3390/rs11030258.

[27] Marinelli, D., Bovolo, F. and Bruzzone, L., (2019). A Novel Change Detection Method for Multitemporal Hyperspectral Images Based on Binary Hyperspectral Change Vectors. *IEEE Transactions on Geoscience and Remote Sensing*, Vol. 57(7), 4913–4928. https://doi.org/10.1109/TGRS.2019.2894339.

[28] Wang, Q., Yuan, Z., Du, Q. and Li, X., (2018). Getnet: A General End-To-End 2-D CNN Framework for Hyperspectral Image Change Detection. *IEEE Transactions on Geoscience and Remote Sensing*, Vol. 57(1), 3–13. https://doi.org/10.1109/TGRS.2018.2849692.

[29] Li, Z., Zhang, H., Li, Z. and Ren, Z., (2022). Residual-Attention Unet++: A Nested Residual-Attention U-Net for Medical Image Segmentation. *Applied Sciences*, Vol. 12(14). https://doi.org/10.3390/app12147149.

[30] Lv, Z., Huang, H., Gao, L., Benediktsson, J. A., Zhao, M. and Shi, C., (2022). Simple Multiscale Unet for Change Detection with Heterogeneous Remote Sensing Images. *IEEE Geoscience and Remote Sensing Letters*, Vol. 19, 1–5. https://doi.org/10.1109/LGRS.2022.3173300.

[31] Zhang, X., Yue, Y., Gao, W., Yun, S., Su, Q., Yin, H. and Zhang, Y., (2021). Difunet++: A Satellite Images Change Detection Network Based on Unet++ and Differential Pyramid. *IEEE Geoscience and Remote Sensing Letters*, Vol. 19, 1–5. https://doi.org/10.1109/LGRS.2021.304937.

[32] Simon, D., (2018). Biogeography-Based Optimization. *IEEE Transactions on Evolutionary Computation*, Vol. 12(6), 702–713.

[33] Bovolo, F., Marchesi, S. and Bruzzone, L., (2011). A Framework for Automatic and Unsupervised Detection of Multiple Changes in Multitemporal Images. *IEEE Transactions on Geoscience and Remote Sensing*, Vol. 50(6), 2196–2212. https://doi.org/10.1109/TGRS.2011.2171493.

[34] Deng, J., Wang, K., Deng, Y. and Qi, G., (2008). PCA-Based Land-Use Change Detection and Analysis Using Multitemporal and Multisensor Satellite Data. *International Journal of Remote Sensing*, Vol. 29(16), 4823–4838. https://doi.org/10.1080/01431160801950162.

[35] Nielsen, A. A., (2007). The Regularized Iteratively Reweighted Mad Method for Change Detection in Multi-and Hyperspectral Data. *IEEE Transactions on Image processing*, Vol. 16(2), 463-478. https://doi.org/10.1109/TIP.2006.888195.

[36] Liu, S., Li, H., Wang, F., Chen, J., Zhang, G., Song, L. and Hu, B., (2023). Unsupervised Transformer Boundary Autoencoder Network for Hyperspectral Image Change Detection. *Remote Sensing*, Vol. 15(7). https://doi.org/10.3390/rs15071868.

[37] Khanbani, S., Mohammadzadeh, A. and Janalipour, M., (2020). Unsupervised Change Detection of Remotely Sensed Images from Rural Areas Based on Using the Hybrid of Improved Thresholding Techniques and Particle Swarm Optimization. *Earth Science Informatics*, Vol. 13(3). https://doi.org/10.1007/s12145-020-00455-8.